

Earth's Future

RESEARCH ARTICLE

10.1029/2023EF003856

Zixuan Zhou and Yong-Tak Kim contributed equally to this work.

Key Points:

- Joint return periods of severity and duration of droughts are compared based on multiple drought indices and climate projections
- Drought index inputting warming trend exclusively captures the emergence of unprecedentedly severe and prolonged droughts
- Climate models with higher warming sensitivity unveil the temperature's effect more explicitly in future projections of droughts

Supporting Information:

Supporting Information may be found in the online version of this article.

Correspondence to:

E.-S. Im and H.-H. Kwon,
ceim@ust.hk;
hkwon@sejong.ac.kr

Citation:

Zhou, Z., Kim, Y.-T., Im, E.-S., & Kwon, H.-H. (2024). Impact of anthropogenic warming on future unprecedented droughts in California: Insights from multiple indices and multi-model projections. *Earth's Future*, 12, e2023EF003856. <https://doi.org/10.1029/2023EF003856>

Received 26 MAY 2023

Accepted 20 DEC 2023

Author Contributions:

Conceptualization: Eun-Soon Im, Hyun-Han Kwon

Data curation: Zixuan Zhou, Yong-Tak Kim

Formal analysis: Zixuan Zhou, Yong-Tak Kim

© 2024 The Authors. *Earth's Future* published by Wiley Periodicals LLC on behalf of American Geophysical Union. This is an open access article under the terms of the Creative Commons Attribution-NonCommercial-NoDerivs License, which permits use and distribution in any medium, provided the original work is properly cited, the use is non-commercial and no modifications or adaptations are made.

Impact of Anthropogenic Warming on Future Unprecedented Droughts in California: Insights From Multiple Indices and Multi-Model Projections

Zixuan Zhou¹ , Yong-Tak Kim^{2,3} , Eun-Soon Im^{1,2} , and Hyun-Han Kwon⁴ 

¹Division of Environment and Sustainability, The Hong Kong University of Science and Technology, Hong Kong, China,

²Department of Civil and Environmental Engineering, The Hong Kong University of Science and Technology, Hong Kong, China, ³Korea Institute of Civil Engineering and Building Technology, Goyang-si, Republic of Korea, ⁴Department of Civil and Environmental Engineering, Sejong University, Seoul, Republic of Korea

Abstract So-called hot droughts are seen as one of the very foreseeable extremes amid the faster-than-expected pace of global warming. In particular, the western part of North America has been pummeled by severe droughts due to a lack of precipitation as well as record-breaking hot temperatures. This study assesses the joint return period of drought severity and duration using the COordinated Regional Climate Downscaling EXperiment-COMmon Regional Experiment (CORDEX-CORE) simulations over the California domain. Six dynamically downscaled simulations with 25 km resolution are analyzed for the historical (1956–2005) and future (2050–2099) periods, whose warming sensitivities differ based on three global climate models (GCMs) driving two regional climate models (RCMs). Our focus is on estimating the joint probabilities of the drought duration and severity constructed from multiple drought indices such as the Palmer Drought Severity Index (PDSI) (with original temperature (PDSI) and its detrended counterpart (PDSI_detrended)) and Standardized Precipitation Index (SPI). Under the RCP8.5 scenario, an unprecedented level of droughts in terms of both duration and severity is likely to emerge only when the drought is characterized by PDSI. A comparison of PDSI and PDSI_detrended explicitly reveals that the occurrence of severe and prolonged droughts is mainly attributed to the warming trend of temperature. Both PDSI_detrended and SPI, which do not incorporate the warming effect explicitly, barely differentiate the joint distributions from the historical and future simulations. Unlike the PDSI based on water budget, the SPI, based on solely accumulated precipitation, shows a loosely coupled joint structure between the severity and duration of droughts, with marked differences in their marginal distributions.

Plain Language Summary Recent mega-droughts in California have enhanced public awareness of hot droughts driven by not only a lack of precipitation but also increased evapotranspiration. While a warmer temperature is expected to exacerbate soil dryness, few studies have attempted to explicitly separate temperature effects on future drought projections. In this regard, a comparative assessment of drought characteristics based on multiple drought indices and climate projections is conducted with a focus on temperature's role in determining drought severity and duration. The unprecedentedly extreme droughts, which have never occurred in both observation and historical simulations, are projected to emerge under the high-emission scenario only when measured by the drought index with the input of both precipitation and temperature. However, when the same index is calculated with the temperature after removing the warming trend, the severity and duration of projected droughts remain mostly unchanged. In addition, the drought index, based on solely accumulated precipitation, does not differentiate the drought characteristics between historical and future simulations. These results demonstrate the significant role of temperature in shaping drought characteristics. If the upward trend of temperature continues, the intensification of severe droughts is very likely to occur even without the changes in precipitation.

1. Introduction

California and much of the Western U.S. have witnessed their third consecutive year of extreme drought in 2022, the driest year to date over the past 128 years (National Drought Mitigation Center et al., 2022; The California Natural Resources Agency et al., 2022). The extended and extreme drought has a devastating impact on water supply (California Department of Water Resources, 2022a) and food production (U.S. Department

Funding acquisition: Eun-Soo Im, Hyun-Han Kwon

Investigation: Zixuan Zhou, Yong-Tak Kim, Eun-Soo Im, Hyun-Han Kwon

Methodology: Zixuan Zhou, Yong-Tak Kim, Eun-Soo Im, Hyun-Han Kwon

Project Administration: Eun-Soo Im, Hyun-Han Kwon

Resources: Eun-Soo Im, Hyun-Han Kwon

Software: Zixuan Zhou, Yong-Tak Kim

Supervision: Eun-Soo Im

Validation: Zixuan Zhou, Yong-Tak Kim

Visualization: Zixuan Zhou, Yong-Tak Kim

Writing – original draft: Zixuan Zhou, Eun-Soo Im, Hyun-Han Kwon

of Agriculture, 2022). Large wildfires in California also greatly impacted the population and the ecosystem (National Oceanic and Atmospheric Administration & National Integrated Drought Information System, 2022).

Record low rainfall and snowpack are probably one primary driver for such a severe drought, according to studies on the 2012–2015 California drought, a similar dry event to the one in 2022 (AghaKouchak et al., 2014; Luo et al., 2017; Mao et al., 2015; Shukla et al., 2015; Williams et al., 2015). The average precipitation amount across the state was only 76% of the year-on-year mean up to October 2022 (California Department of Water Resources, 2022a). Meanwhile, the snowpack that serves as a key component of the water supply was only 38% of the past years' average on 1 April 2022, a time when it should have been its deepest (California Department of Water Resources, 2022b). Although moisture deficiency constitutes an important prerequisite for drought (Dai, 2011; Diffenbaugh et al., 2015), the warmer temperatures greatly exacerbate California's drought by enhancing evapotranspiration demand and depleting available soil moisture (Allen & Anderson, 2018; Cook et al., 2014; Dai et al., 2004; Diffenbaugh et al., 2015; Easterling et al., 2007; Kew et al., 2021; Rind et al., 1990; Trenberth et al., 2014). January through August 2022 ranks California's fifth warmest year, following 2021's warmest summer on record (Becker, 2022). Temperatures were above normal across the entire West, with many long-term stations in the top five warmest summers (National Oceanic and Atmospheric Administration & National Integrated Drought Information System, 2022).

While numerous studies examine droughts purely based on precipitation change, more and more literature acknowledges that ignoring the rising temperature's effect in aggravating droughts will lead to a severe underestimation of drought risk (AghaKouchak et al., 2014; Cai et al., 2009; Diffenbaugh et al., 2015; Easterling et al., 2007; Griffin & Anchukaitis, 2014; Im et al., 2012; Kelley et al., 2015). By analyzing historical climate observations, Diffenbaugh et al. (2015) find that the probability of drought in California more than doubles if precipitation deficits co-occur with warm conditions. AghaKouchak et al. (2014) reveal that the recurrence interval for the 2014 California drought increased from approximately 24 years when only considering precipitation to 200 years upon inclusion of temperature. The unprecedented severity of the 2007–2010 Syria drought is also found to be highly unlikely without the long-term warming trend (Kelley et al., 2015). With a continuously warming climate (Cook et al., 2014), the temperature is expected to sustain its effect in intensifying drought. It might be a crucial factor to consider when assessing future droughts.

This study investigates the impact of increased temperature on drought severity and duration in California using multiple climate models and drought indices. Two main factors that make drought assessment uncertain are examined. First, although climate models generally agree on temperature increase, the warming magnitude still depends on different models' warming sensitivity, which can lead to divergent drought projections (Beniston et al., 2007; Houghton et al., 2001; Knutti et al., 2002; Räisänen, 2007). Meanwhile, the selection of a drought index can be a significant source of uncertainty in the drought assessment due to the use of multiple meteorological variables that may represent mixed effects on defining different types of droughts even under the same conditions (Lee et al., 2019; Reyniers et al., 2023; Rhee & Cho, 2016; Satoh et al., 2021; Sutanto & Van Lanen, 2021; Touma et al., 2015; Trenberth et al., 2014). This study adopts two common drought indices, the Palmer Drought Severity Index (PDSI) (Palmer, 1965) based on both temperature and precipitation, and the Standardized Precipitation Index (SPI) informed by precipitation solely. PDSI_detrended with the detrended temperature is also included in the comparison to discern the effect of temperature. A copula function combining marginal distributions for the drought variables (e.g., duration and severity) is mainly employed to analyze the bivariate probability of the drought severity and duration over historical and future periods. By systematically comparing the drought assessed by different climate models and drought indices, this study aims to offer insights into the contribution of temperature to the change in the drought return period over different periods under climate change with a demonstration of the uncertainty stemming from drought indices.

2. Data and Method

2.1. Multi-GCM and Multi-RCM Climate Projections

In this study, monthly mean temperature (°C) and precipitation (mm/day) for the historical period (1956–2005) and future period (2050–2099, forced under Representative Concentration Pathway 8.5) were acquired from Coordinated Regional Climate Downscaling EXperiment-COMmon Regional Experiment (CORDEX-CORE; Giorgi et al., 2021) data set over the North American region (NA-CORDEX; Mearns et al., 2017) at a spatial resolution

Table 1
Model Full Names, Key References, and Models' Abbreviated Names Used in This Study

GCM	Full Name	Reference	Abbrev.
GFDL-ESM2M	Geophysical Fluid Dynamics Laboratory-Earth System Model	Dunne et al. (2012, 2013)	GFDL
MPI-ESM-LR	Max Planck Institute-Earth System Model	Giorgetta et al. (2013)	MPI
HadGEM2-ES	Hadley Centre Global Environment Model version 2	Collins et al. (2011)	HadGEM
RCM	Full Name	Reference	Abbrev.
RegCM4	The Regional Climate Model system version 4	Giorgi et al. (2012)	RegCM
WRF	Weather Research & Forecasting Model	Skamarock et al. (2019)	WRF

of 25 km. The dynamically downscaled results from two Regional Climate Models (RCMs) driven by three Global Climate Models (GCMs) from Coupled Model Intercomparison Project 5 (CMIP5; Taylor et al., 2012) were compared. The data has been bias-corrected using a multivariate bias correction algorithm (Cannon, 2018) against the Gridded Surface Meteorological Dataset (gridMET; Abatzoglou, 2013), an observation-based grid climate data set including precipitation and temperature. To investigate the added value of dynamic downscaling, monthly mean temperature and precipitation data were retrieved from the driving GCMs, which were then interpolated to the RCM grid using a bilinear interpolation technique to align with the RCM data. The model names, key references, and abbreviations used in this article are summarized in Table 1.

2.2. Gridded Observed Temperature and Precipitation Data

To validate the historical simulation, monthly observed mean temperature (°C) and precipitation (mm/month) data were retrieved from the fourth version of the Climatic Research Unit gridded Time Series monthly high-resolution gridded multivariate climate data set (CRU TS v4; Harris et al., 2020) provided by Climatic Research Unit (University of East Anglia) and Met Office. The observation data set covers the North American domain on a 0.5° latitude by 0.5° longitude grid and spans 1901–2021. Major considerations for this selection are: (a) the data set covers the historical period of the simulation data; (b) its spatial resolution is close to that of the simulation data. To ensure a consistent comparison at the same spatial resolution, observed temperature and precipitation data were interpolated to the RCM grid using a bilinear interpolation technique.

2.3. Drought Indices and Drought Definition

Two drought indices, PDSI and SPI, were computed on a monthly basis to characterize the spatial and temporal variations of drought in California during the historical period (1956–2005) and future period (2050–2099). Besides the temperature and precipitation data from model simulations, the detrended temperature series of RCM simulated data was used for the estimation of PDSI to better understand the role of the temperature in drought assessment in a more explicit manner. As a result, there are a total of three sets of indices derived by using different combinations of climate inputs: (a) PDSI calculated with precipitation and original temperature without detrending; (b) PDSI calculated with precipitation and detrended temperature (referred to as PDSI_detrended hereafter); and (c) SPI calculated with precipitation only.

PDSI is usually considered an index of meteorological drought (Burke et al., 2006; Diffenbaugh et al., 2015) and has been widely used to quantify drought in the literature (Burke et al., 2006; Cook et al., 2015; Dai, 2013; Lehner et al., 2017; Trenberth et al., 2014). The index is based on a soil moisture balance model, which considers the inflow of moisture into the soil (primarily from precipitation) as well as the outflow of moisture from the soil (primarily as a result of evapotranspiration). It is normalized at a local scale relative to a baseline period in a given location, with negative values indicating drier than normal conditions (droughts) and positive values indicating wetter than normal conditions (pluvials) (Cook et al., 2014). In our study, a drought starts when the PDSI anomalies are continuously under -1 and ends when PDSI anomalies become above -1 . Under this definition, the drought variables (or characteristics), such as drought duration and severity, can be formally obtained from the PDSI anomalies for the exploration of changes in joint return periods over historical and future periods. However, it is noteworthy that PDSI simply reflects drought variability from a context of water budget rather than socio-hydrological factors such as human water demand, stream flow, reservoir storage, or accessibility

of groundwater (Williams et al., 2015). To derive the PDSI series, more specifically, monthly temperature and precipitation values were used to compute potential evapotranspiration (PET) by the Thornthwaite method (Thornthwaite, 1948), which was then fed to a simplified soil moisture balance model for the derivation of the net moisture balance. Following the same procedure, PDSI_detrended was calculated by using precipitation and detrended temperature, which removed the warming trend from 1956 to 2099. The PET estimates can vary depending on the methods, and critics of the Thornthwaite method suggest that it potentially overestimates the PET, leading to frequent drought states because of its dependence on surface temperature (Sheffield et al., 2012). However, it has been found that the choice of methods in the calculation of PET does not critically influence the outcome of historical PDSI estimates in the vicinity of California (Dai, 2011; Diffenbaugh et al., 2015; Sheffield et al., 2012; Van der Schrier et al., 2011).

SPI, a precipitation anomaly series that deviated from the long-term climatology, was used to assess meteorological drought for the purpose of comparison with those of PDSI. SPI was developed by McKee et al. (1993) and is a well-established meteorological drought index widely adopted in various studies (e.g., Ahmadalipour et al., 2017; Lee et al., 2019). A negative SPI value denotes below-normal precipitation, indicating the start of a drought in this study. We calculated SPI on a 12-month timescale. First, the accumulated precipitation series for a moving window of 12 months over a historical period were obtained. Next, the precipitation deficits were computed by subtracting the historical mean and then fitted to a gamma distribution, as proposed in previous studies (McKee et al., 1993; Stagge et al., 2015; Touma et al., 2015). The cumulative probability of the gamma distribution was then transformed into a standard normal function (with a mean of 0 and standard deviation of 1), which would be the value of the SPI. The parameters of the gamma distribution were estimated based on the historical data through a maximum likelihood method, and the same methodology was used for future drought projections.

2.4. Joint Return Period Estimation Using Copulas

This study adopts Copulas to explore changes in joint return periods of bivariate random variables, taking advantage of the separation in the modeling between dependence structure and marginal distributions of the drought variables (i.e., drought duration and severity). First, this study considered the goodness-of-fit (GoF) tests based on the negative log-likelihood and the Bayesian information criterion for the selection of the marginal distributions of the variables. The two-parameter Lognormal distribution and the two-parameter Gamma distribution were identified as the marginal distributions for the drought duration (d_1) and severity (d_2) constructed from drought indices (i.e., PDSI, PDSI_detrended, and SPI), respectively (Table S1 in Supporting Information S1).

$$f(d_1) = \frac{1}{d_1\sigma\sqrt{2\pi}} \exp\left(-\frac{(\log(d_1) - \mu)^2}{2\sigma^2}\right) \quad (1)$$

$$f(d_2) = \frac{d_2^{\alpha-1} \exp(-\beta d_2)}{\beta^\alpha \Gamma(\alpha)} \quad (2)$$

where, μ and σ in Equation 1 are the mean and standard deviation of the drought duration's (d_1) natural logarithm, whereas α and β in Equation 2 are the shape and scale parameter of the gamma distribution for the drought severity (d_2), respectively.

The log-likelihood was calculated for the four copulas (Gaussian, Clayton, Frank, and Gumbel) under the same marginal distributions (Table S2 in Supporting Information S1), and the Gaussian copula was selected for PDSI and SPI. Since a closed functional form of the Gaussian copula is not readily available analytically, the Gaussian copula can then be constructed from a multivariate Gaussian distribution in the context of the probability integral transform, as follows (Copula parameters | 0.81 for PDSI and PDSI_detrended and 0.58 for SPI):

$$C(u, v) = \int_{-\infty}^{\Phi^{-1}(u)} \int_{-\infty}^{\Phi^{-1}(v)} \frac{1}{2\pi(1-\rho^2)^{1/2}} \exp\left\{-\frac{d_1^2 - 2\rho d_1 d_2 + d_2^2}{2(1-\rho^2)}\right\} dx dy \quad (3)$$

where Φ^{-1} is the inverse of a standard normal cumulative distribution function.

$$u = F_{d_1}(d_1) \quad (4)$$

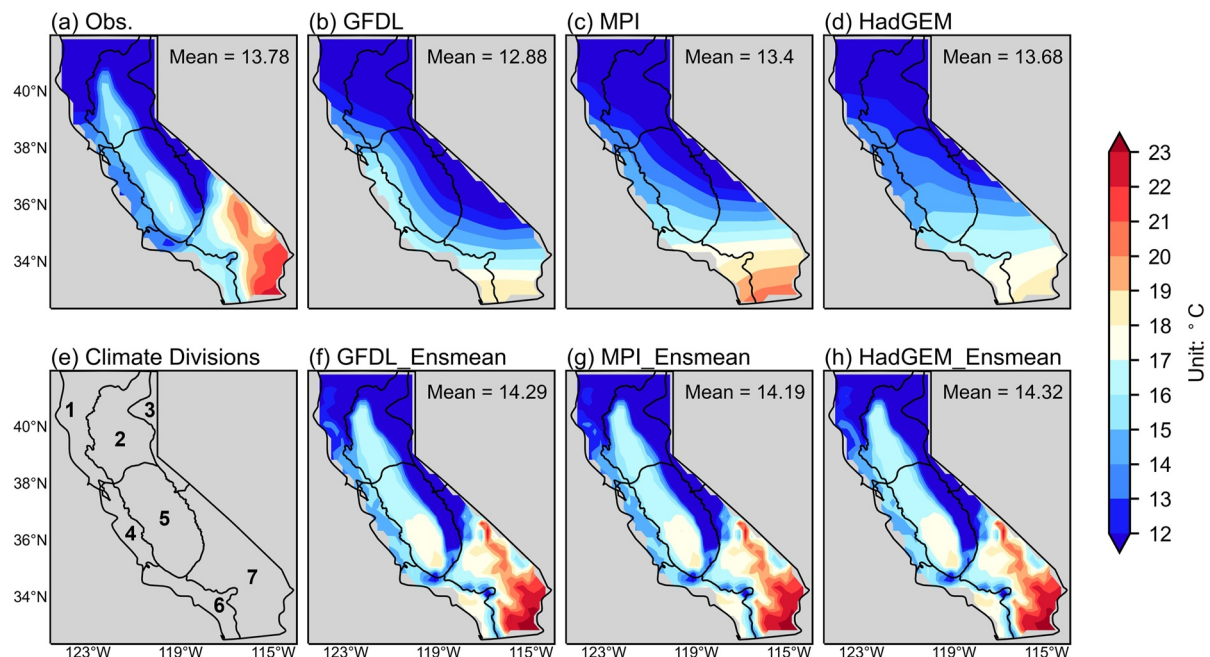


Figure 1. Spatial distribution of 50-year climatological Tmean in the historical period (1956–2005), based on Observation (a), Global Climate Model (b–d), and Regional Climate Model (RCM) ensemble mean (f–h; average of RegCM and WRF). The mean value in each graph indicates the spatially averaged Tmean. All the data were interpolated onto the 25 km grid (i.e., the grid of RCM) before calculation. Subplot (e) shows the generally recognized California climate divisions (from National Oceanic and Atmospheric Administration/National Centers for Environmental Information websites: <https://psl.noaa.gov/data/usclimdivs/boundaries.html>): 1-North Coast Drainage, 2-Sacramento Drainage, 3-Northeast Interior Basins, 4-Central Coast Drainage, 5-San Joaquin Drainage, 6-South Coast Drainage, 7-Southeast Desert Basins. The climate divisions are overlaid as black lines on all subplots.

$$v = F_{d_2}(d_2) \quad (5)$$

where, F_{d_1} and F_{d_2} indicate the marginal cumulative density function for the drought duration (d_1) and severity (d_2), respectively.

The joint return period (T) between the drought duration and severity, with the mean time interval $M(L)$ between the drought events, can be formulated as follows:

$$T = \frac{M(L)}{P(D_1 \geq d_1, D_2 \geq d_2)} = \frac{M(L)}{1 - F_{d_1}(d_1) - F_{d_2}(d_2) + C(F_{d_1}(d_1), F_{d_2}(d_2))} \quad (6)$$

3. Results

3.1. Validation of Historical Simulations

The climatological pattern of mean temperature (Tmean) and precipitation, which are primary variables used for the calculation of drought indices, were first explored to validate model performance over the historical period. Figures 1 and 2 illustrate the spatial distributions of the 50-year averaged Tmean and precipitation during the historical period (1956–2005), respectively. The RCM ensemble mean is equivalent to the average of two RCMs: RegCM and WRF. For comparison purposes, in-situ observational data and the original GCM data were interpolated into the same 25 km grid as the RCMs, using the bilinear remapping function in Climate Data Operators programming. It is worth noting the RCM values are bias-corrected, which leads to their reduced inter-model variability during the historical period.

The statewide mean of observed Tmean (Figure 1a) is roughly similar to that of GCM (Figures 1b–1d) and RCM ensemble mean (Figures 1f–1h), although three RCM ensemble means are on average slightly warmer by 0.4–0.5 degree Celsius. Using the widely recognized National Oceanic and Atmospheric Administration/National Centers for Environmental Information (NOAA/NCEI) California Climate Divisions (NOAA National Centers

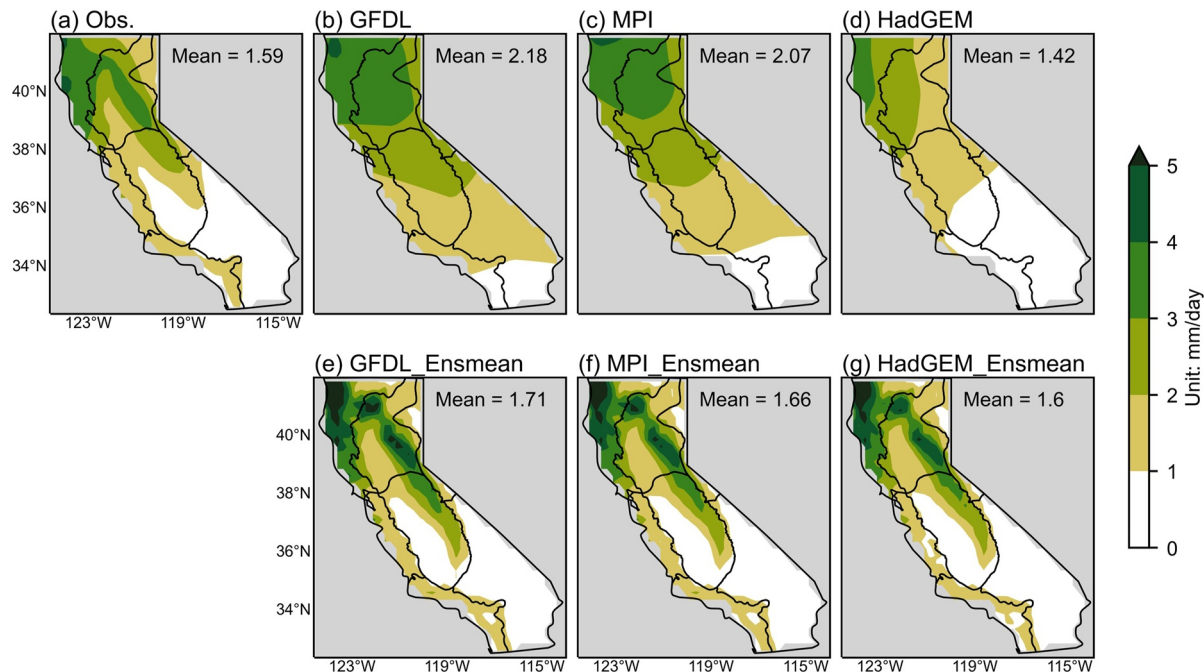


Figure 2. As in Figure 1, but for precipitation patterns based on Observation (a), Global Climate Model (b–d), and Regional Climate Model ensemble mean (e–g; average of RegCM and WRF). The black lines resemble the boundaries of seven climate divisions defined in Figure 1.

for Environmental Information, 2023), we divided California into seven regions to characterize the sub-regional patterns in a clearer way. The observed spatial distribution of Tmean roughly describes the topographical pattern. For instance, Tmean (Figure 1a) is distinctively higher in Division 7, near the Mojave Desert, and lower on the Sierra Nevada Mountain that goes across Division 2 and 5. The map is also characterized by a blue oval shape in Division 2 and 5, representing the warm Great Valley region. Such sub-regional patterns are effectively represented by the RCM simulations but obfuscated by GCMs. Specifically, in Division 2 and 5, the RCMs (Figures 1f–1h) capture the sharp drop in temperature from the mountain to the Great Valley, whereas the GCMs only render an unrefined temperature gradient following the latitudinal changes.

As for precipitation, the statewide mean of two GCMs—GFDL and MPI—are nearly 30% higher (Figures 2b and 2c), whereas the statewide average of RCM ensemble means (Figures 2e–2g) is close to the statewide observed mean, with an effective reduction in the wet bias presented by GCMs. Meanwhile, the observed map of annual precipitation climatology (Figure 2a) depicts high precipitation in Division 1, 2, 3, and dry condition in Division 5, and 7. However, GCMs obscure such regional details because their resolution is too coarse to resolve local climate patterns (Giorgi & Gutowski, 2016; Qiu & Im, 2021; Qiu et al., 2020; Walton et al., 2020). GCM simulations only produce rough spatial patterns of temperature and precipitation that change from the southeast to the northwest. In contrast, the dynamically downscaled results through WRF and RegCM, benefitting from its higher-resolution surface boundary conditions, well capture the topographically modulated observation patterns, including large rainfall amount in the mountain and warm conditions in the Great Valley, which attests to the added value of downscaling.

Although the analysis of the mean climatology of temperature and precipitation can show the gross features of model performance, it does not directly reveal how Tmean and precipitation translate into drought characteristics because of the non-linear relationship between meteorological variables and drought characteristics (or patterns). Therefore, we also compare the PDSIs obtained from the observed data and model simulations during the historical period to examine the models' capability in representing the observed drought. Figure 3 shows the frequency distributions of PDSI values based on observations, GCM, and RCM simulation data in the historical period (1956–2005). It can be seen that the general shapes of frequency distributions (or histograms) based on GCM PDSI and RCM PDSI are almost identical. While the PDSI computed from GCM and RCM data are both roughly consistent with that of the observed, the frequencies of the RCM-based PDSIs are largely close to the observed PDSI.

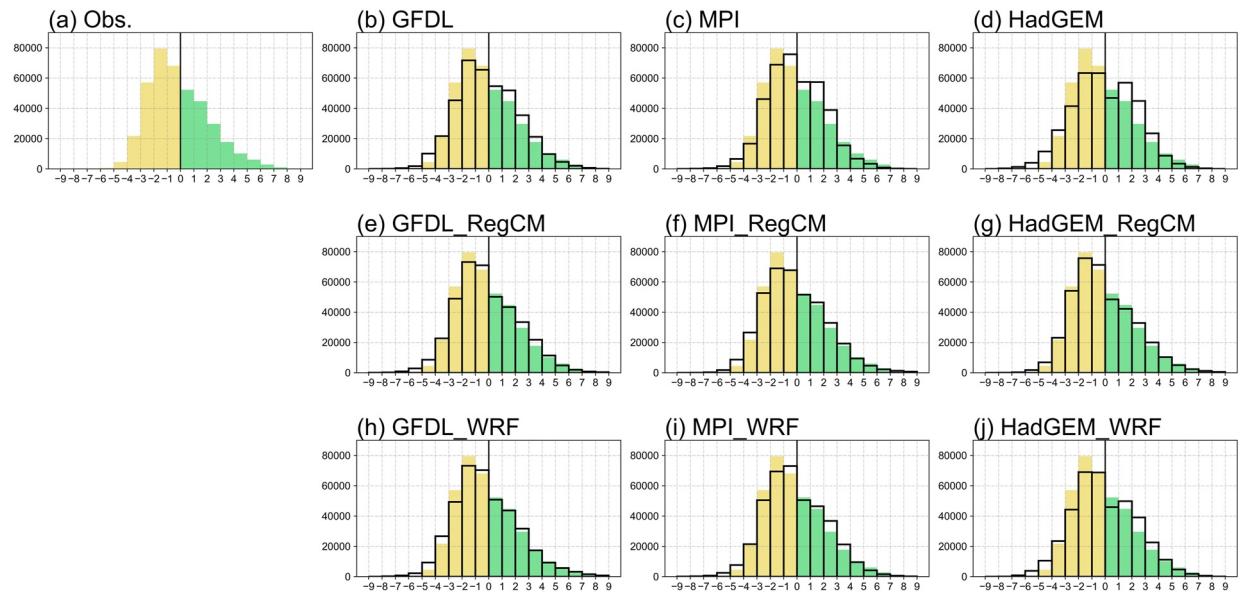


Figure 3. Histograms representing the frequency distribution of PDSI value in the historical period (1956–2005), based on Observation (a), Global Climate Model (GCM) (b–d), and Regional Climate Model (RCM) (e–j) data. The colored bars represent the observed PDSI distribution, while the black lines are the frequency of PDSI calculated by respective GCMs or RCMs.

To further compare the GCM and RCM capability in capturing the observed drought extremes, the spatial distribution of the 50-year average of $\text{PDSI} \leq -4$ in the historical period is illustrated in Figure 4. According to the figure, the area average PDSI of GCM and RCM data are similar, but the spatial distribution of the RCM-based PDSI has distinctly higher coherence to the observed PDSI extremes, including the less extreme drought at Sierra Nevada Mountains, and more severe extremes in the Great Valley region. To illustrate the quantitative aspects of added value of downscaled simulations, we examine the performance of GCMs and RCMs based on sub-regions

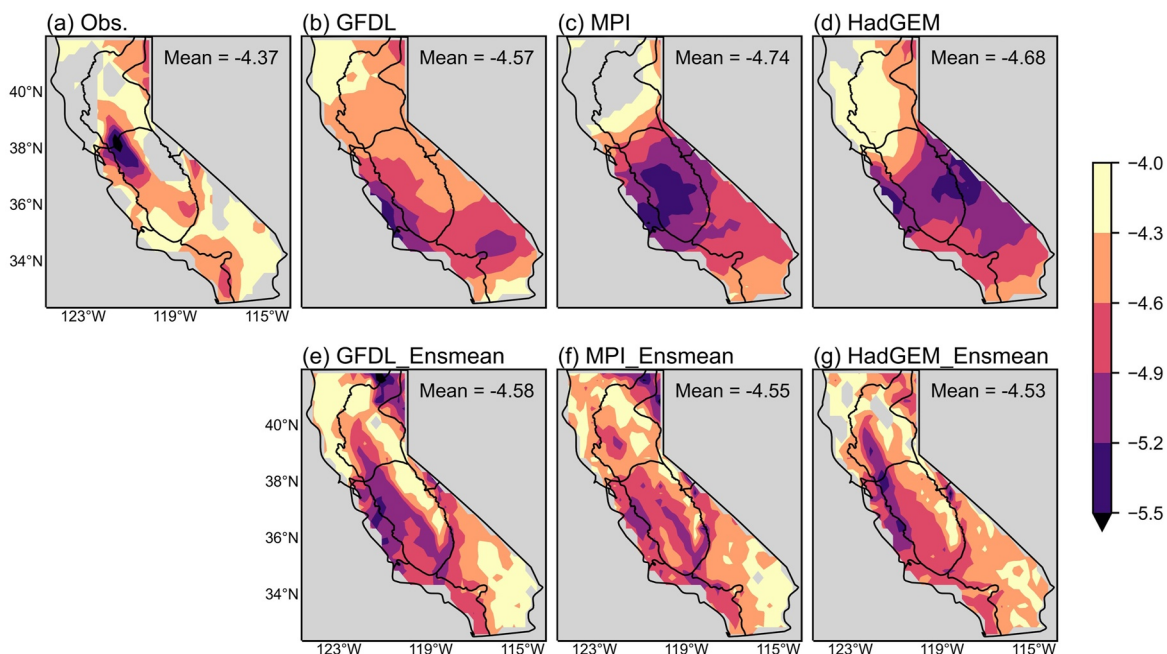


Figure 4. Spatial distribution of the climatological mean of $\text{PDSI} \leq -4$ in the historical period (1956–2005), based on Observation (a), Global Climate Model data (b–d), and Regional Climate Model ensemble mean (e–g; average of RegCM and WRF). The black lines resemble the boundaries of seven climate divisions defined in Figure 1.

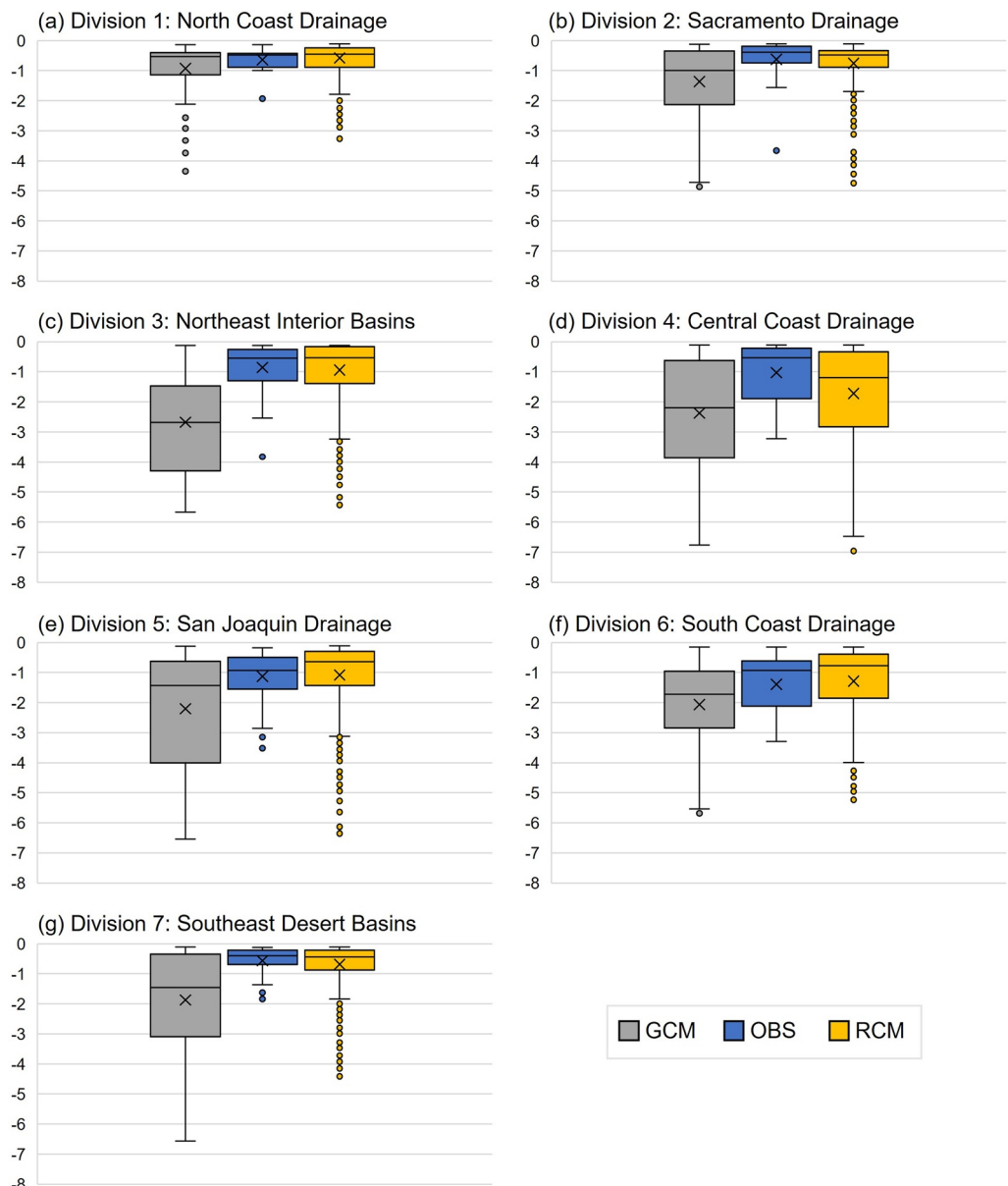


Figure 5. Distribution of extreme drought condition ($\text{PDSI} \leq -4$) in seven climate divisions of California. The value here is the sum of extreme PDSI in each division divided by the number of total gridpoints of the division.

of California. Each climate division's extreme PDSI (under -4) are summed up and divided by the number of gridpoints in each division to ensure a scaled comparison. These values are then pooled together for each month of the study period to calculate the descriptive statistics of extreme drought conditions in each sub-region. The resulting boxplots in Figure 5 show that the San Joaquin Drainage (5e) and South Coast Drainage (5f) exhibit significantly drier conditions compared to the other regions, consistent with previous studies (He & Gautam, 2016). Furthermore, the RCMs demonstrate superior performance in capturing the mean level and inter-month variability of observed extreme droughts compared to GCMs. This again supports that the dynamically downscaled climate data improves the characteristics of local climate patterns, leading to a more refined understanding of droughts.

3.2. Projections of Temperature and Precipitation

Moving to how temperature and precipitation will vary under the future scenarios, Figures 6 and 7 show the prospective changes in Tmean and precipitation, which is calculated by the 50-year future mean (2050–2099)

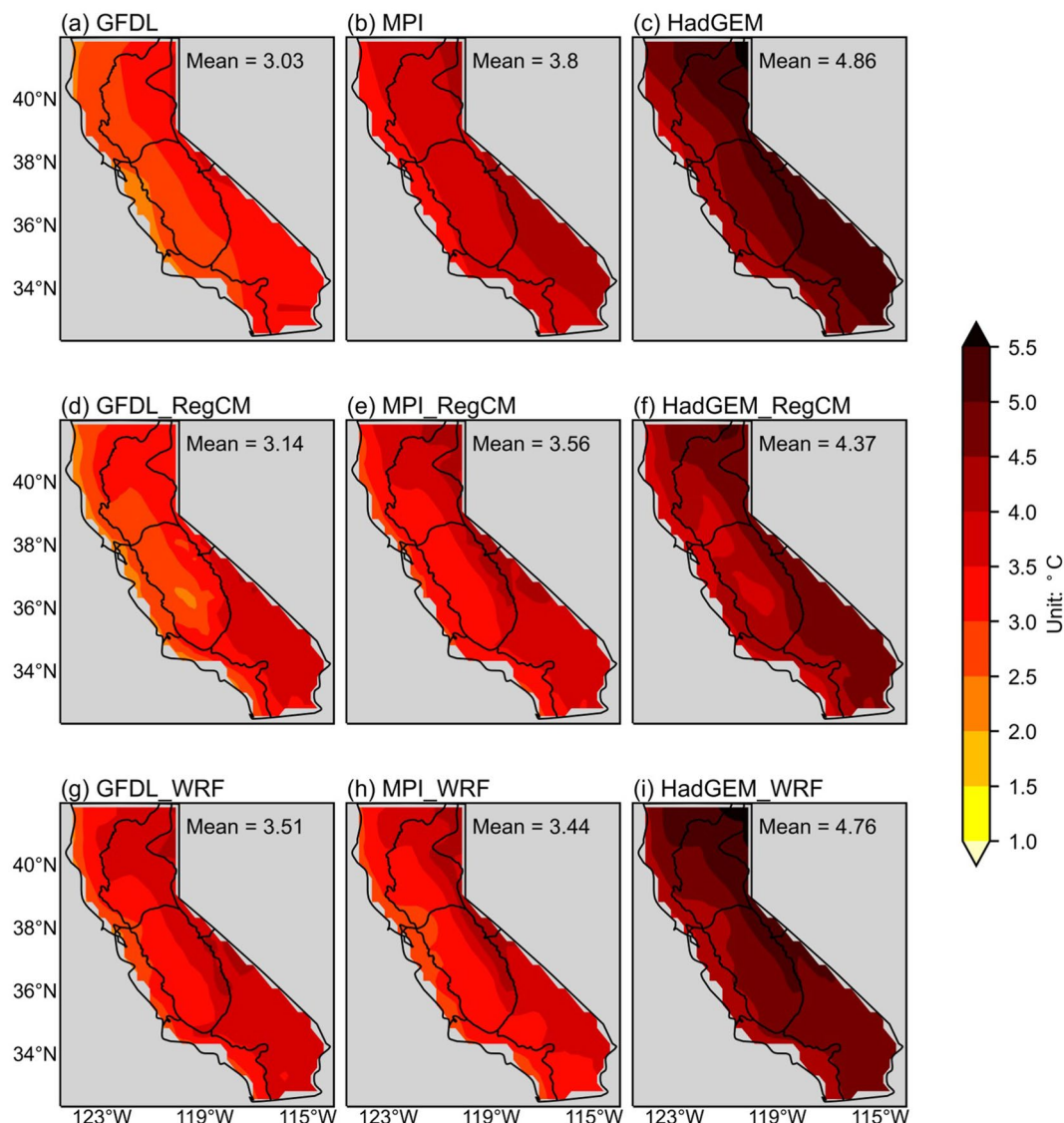


Figure 6. Temperature changes calculated by future 50-year mean (2050–2099; under RCP8.5) minus historical 50-year mean (1956–2005). The first row presents Global Climate Model projections (a–c), while the following two rows present Regional Climate Model projections (d–i). The mean value represents the spatial average of each map. The black lines resemble the boundaries of seven climate divisions defined in Figure 1.

minus the 50-year historical mean (1956–2005). As shown in Figures 6a–6c, all GCMs unequivocally report the temperature increase in the California domain but with different warming magnitudes, with GFDL being the smallest, MPI in the middle, and HadGEM being the largest, which is consistent with the inherent climate sensitivity of each GCM (Bukovsky & Mearns, 2020; Flynn & Mauritzen, 2020). The RCM projections (Figures 6d–6i) largely inherit the changes expected in GCMs, with GFDL_RegCM providing the coolest projections and HadGEM_WRF giving the hottest. Although the downscaled results of MPI and HadGEM both show a small decrease in state-mean temperature change, RCMs driven by GFDL actually project a subtly hotter future than the GCM, mainly in the southeastern desert region and part of the Sierra Nevada Mountain. Furthermore, the temperature anomaly in WRF is almost always warmer than RegCM, except for the GFDL. Such characteristics have also been found in other CORDEX-NA-based studies and are likely to be caused by the differences in the configurations of RCMs (Bukovsky & Mearns, 2020).

Unlike temperature, future precipitation changes are very uncertain and model-dependent. This may be because of the model's internal variability that becomes more important at smaller spatial scales (Hawkins & Sutton, 2009)

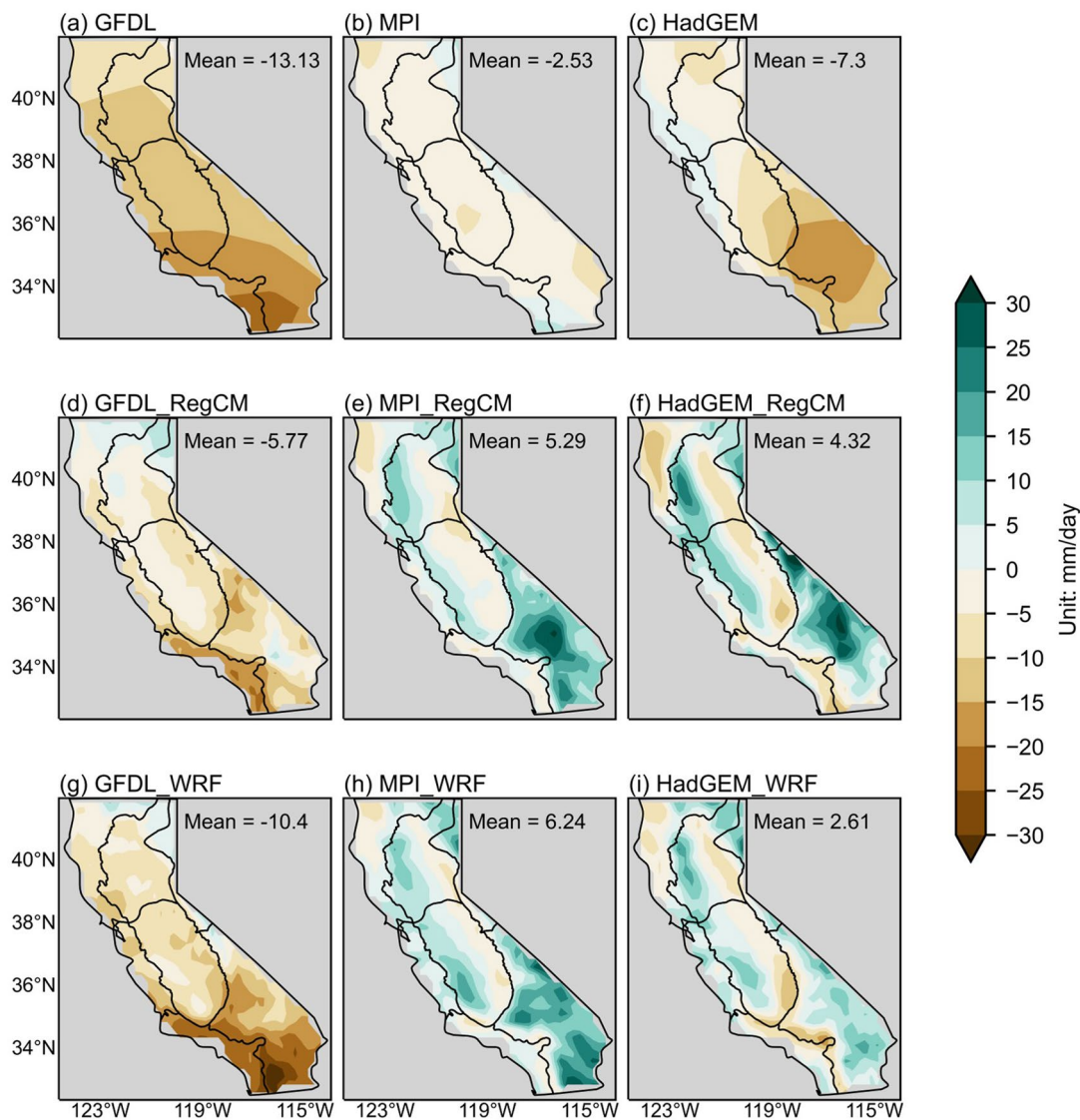


Figure 7. As in Figure 6, but for the percentage changes in precipitation.

and the model uncertainty brought by different combinations of GCMs and RCMs (Bukovsky & Mearns, 2020; Giorgi & Gutowski, 2016; Kim et al., 2020). In addition, the relationship between rainfall changes and model sensitivity remains obscure based on our selected timescale and models, which is also found by Bukovsky and Mearns (2020). Although increased atmospheric moisture holding capacity under warming scenarios could lead to larger precipitation extremes (Trenberth et al., 2007), the rainfall-temperature relationship is affected by several factors such as weather types and locations (Magan et al., 2020; Tie et al., 2023) and highly dependent on the spatial scale and seasons examined (Bukovsky & Mearns, 2020), which all result in the complex relationship between precipitation and model warming sensitivity. Based on statewide averages, all GCM projections show an overall precipitation reduction (Figures 7a–7c) in future periods, with GFDL projecting the most significant rainfall decrease (-13.13%) while MPI projecting the least (-2.53%). Although GFDL_RegCM and GFDL_WRF (Figures 7d and 7g) closely resemble the precipitation change from the GCM, the RCM projections driven by MPI (Figures 7e and 7h) and HadGEM (Figures 7f and 7i) have a strong wetting signal in Division 7 as opposed to the drying projected by the driving GCMs, which is possibly a result of the different physics representations in the models (Giorgi & Gutowski, 2016). This study examined previous studies and validated such a trend of precipitation increase in RCMs, albeit some investigated slightly different periods as well as broader spatial scales (Bukovsky & Mearns, 2020; Hughes et al., 2022; Meyer et al., 2021; Teichmann et al., 2021).

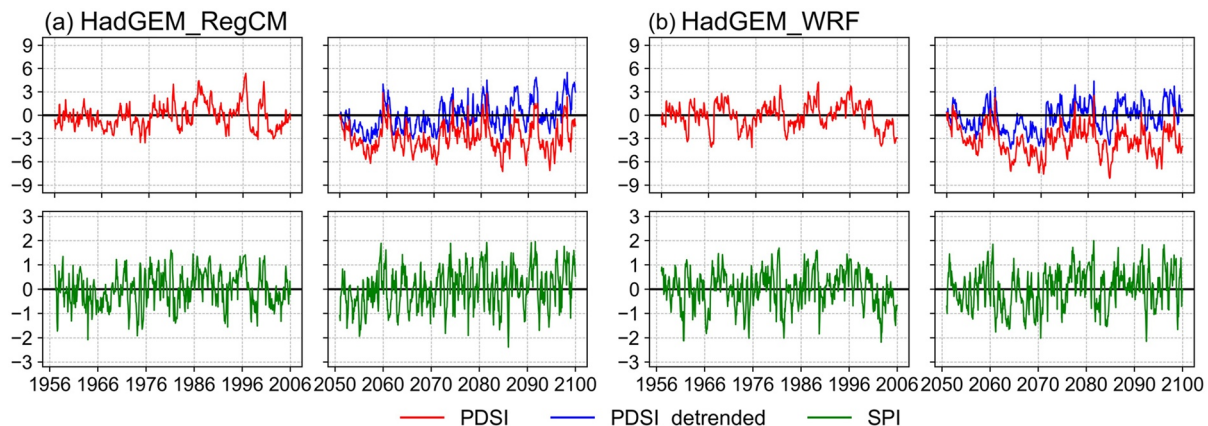


Figure 8. Time series of PDSI, PDSI_detrended, and SPI based on HadGEM_RCM Tmean (detrended Tmean for PDSI_detrended) and precipitation data during the historical period (1956–2005) and future period (2050–2099; under RCP8.5).

3.3. The Effect of Temperature on Future Drought Characteristics

To measure the temporal evolution of drought conditions varying across different indices, the monthly time series of PDSI, PDSI_detrended, and SPI, averaged over the California domain based on two RCMs driven by HadGEM, are illustrated in Figure 8. The time series of all models involved in this study are presented in Figure S1 in Supporting Information S1. According to Figure 8 and other models in Figure S1 in Supporting Information S1, PDSI has a distinct decreasing trend. Alternatively, both PDSI_detrended, which removes the warming trend, and SPI, which only incorporates precipitation changes, have an insignificant tendency in future periods. The downward trend of PDSI is likely a result of enhanced evapotranspiration under future warming (Dai et al., 2004), which is in line with those found in other research (Bonsal et al., 2013; Im et al., 2012). Such results indicate that the warming temperature plays a key role in exacerbating future droughts, substantiating the effectiveness of PDSI in understanding the warming effect in a changing climate. However, it is worth noting that the results here do not mean to downgrade SPI's ability to assess drought. Generally, SPI is considered to be more suitable for humid regions where it experiences high rainfall, whereas PDSI can be utilized to capture drought characteristics effectively in dry or semiarid regions where PET is one of the dominant factors in hydrological circulation (Pathak & Dodamani, 2020; Yang et al., 2017). Therefore, in California, characterized by low precipitation and high evapotranspiration demand, SPI may not be comprehensive enough to capture drought characteristics and depict future drought aggravation induced by warming due to the absence of a moisture depletion process from the surface to the atmosphere.

The impact of temperature on future drought seen in the time series of PDSI is also delineated in the joint return period of drought duration and severity. Figure 9 shows the joint return period of PDSI estimated from six dynamically downscaled simulations. To begin with, the recent observation of the 2022 California drought (yellow star) has a return period of 100 years from the statistical point of view, which means that a drought of similar duration and severity has a 1% chance of being exceeded in any one year under the current climate conditions. The rarity of this event is well demonstrated by the distance of the yellow star from the blue star, which indicates the return period (i.e., location) corresponding to the observed mean duration and severity. Under the RCP8.5 scenario, the mean return values (i.e., red star) projected from all GCM-RCM chains are positioned much closer to the historical extreme (i.e., yellow star) compared to historical mean values (i.e., green star). It implies that statistically rare events like the 2022 California drought are expected to be the new norm if the global emission pathway follows the RCP8.5 scenario. More importantly, the unprecedentedly extreme droughts (e.g., mega-drought) that have never occurred in both observation and historical simulations are likely to emerge, and this is a consistent pattern across all projections. The return period of the mega-drought events, given the current climate, is estimated to be nearly 500–2000. Next, comparing individual model characteristics based on the mean of the duration and severity obtained from climate models (red star) and distribution bounded by 90% of data (i.e., red elliptic curve), HadGEM-driven RCMs are likely to report more exacerbated future drought than MPI-driven RCMs, whereas RCMs driven by MPI and HadGEM commonly show an increase in precipitation in the future. Therefore, it is the case that models with higher warming sensitivity could lead to more severe and prolonged droughts. Meanwhile, it is also confirmed that decreases in precipitation exacerbate future droughts. If GFDL_WRF and HadGEM_WRF (Figures 9d and 9f) are compared,

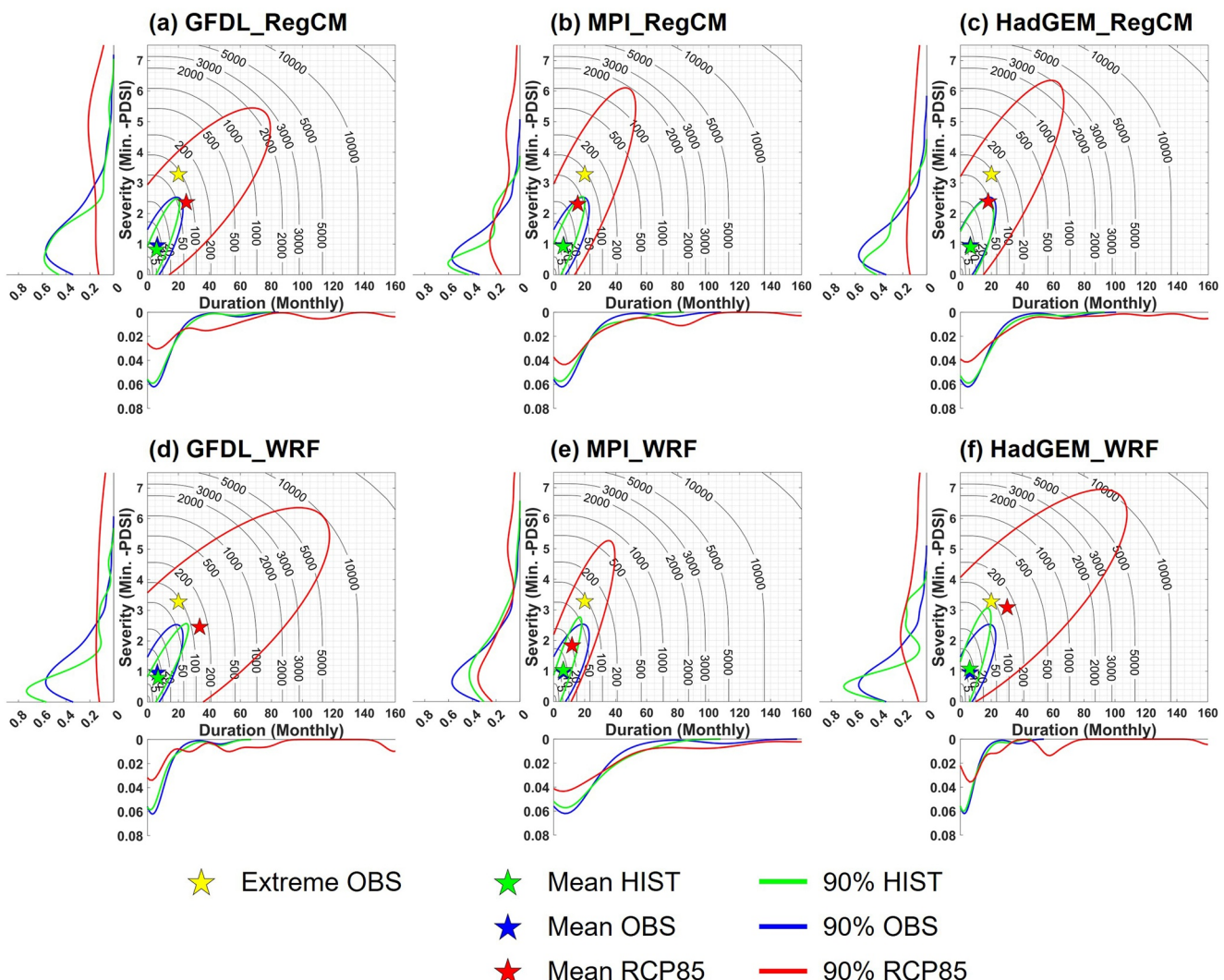


Figure 9. Joint return periods (T) of drought severity (S) and duration (D) estimated based on state-wide average PDSI, which is formulated as $T(D \geq d \text{ and } S \geq s)$. The numbered curves inside each graph indicate the number of years for return periods T . The yellow star is the recently observed extreme drought in 2022, the blue star is the mean of observed drought, and the green and red stars are the mean of historical droughts and future droughts under the RCP8.5 scenario, respectively. The green, blue, and red ecliptic lines resemble the distribution bounded by 90% of the data during the corresponding period. Near the two axes are the marginal density curves representing the frequency distribution of drought duration (near x-axis) or severity (near y-axis). Figure S2 in Supporting Information S1 presents the detailed distribution of each drought event as colored scatter dots (Observation-blue, Historical-green, RCP85-red).

the mean of the duration and severity for the future period, which does not exist inside the distributions of both the observation and simulations over the historical period, appeared in a similar location, even though GFDL_RegCM has the least warming and HadGEM_RegCM has the most (Figure 6). This may be because GFDL_RegCM projects the largest drying (Figure 7), whereas the future projection of HadGEM_RegCM shows an increase in precipitation in many areas across the state. The precipitation deficit in GFDL_RegCM is likely to compensate for the lower warming magnitude and lead to similar future drought states with models that project a warmer and wetter climate in the future.

The joint return periods estimated based on state mean PDSI_detrended and SPI are illustrated in Figures 10 and 11, respectively. Since the trend of temperature is not dominant during the historical period, the mean return period from PDSI_detrended in Figure 10 is not noticeably different from PDSI shown in Figure 9. However, PDSI_detrended under the RCP8.5 scenario, which is calculated with temperature after removing a strong warming trend, shows an entirely different behavior. In contrast to the PDSI, the joint distribution bounded by 90% of data significantly shrinks, only retaining minimal changes in their shape from that of the historical period. Indeed, PDSI_detrended projects future marginal distributions of severity and duration to be almost identical to the historical ones. However, the marginal distributions of severity and duration from PDSI shift substantially toward the higher values in the

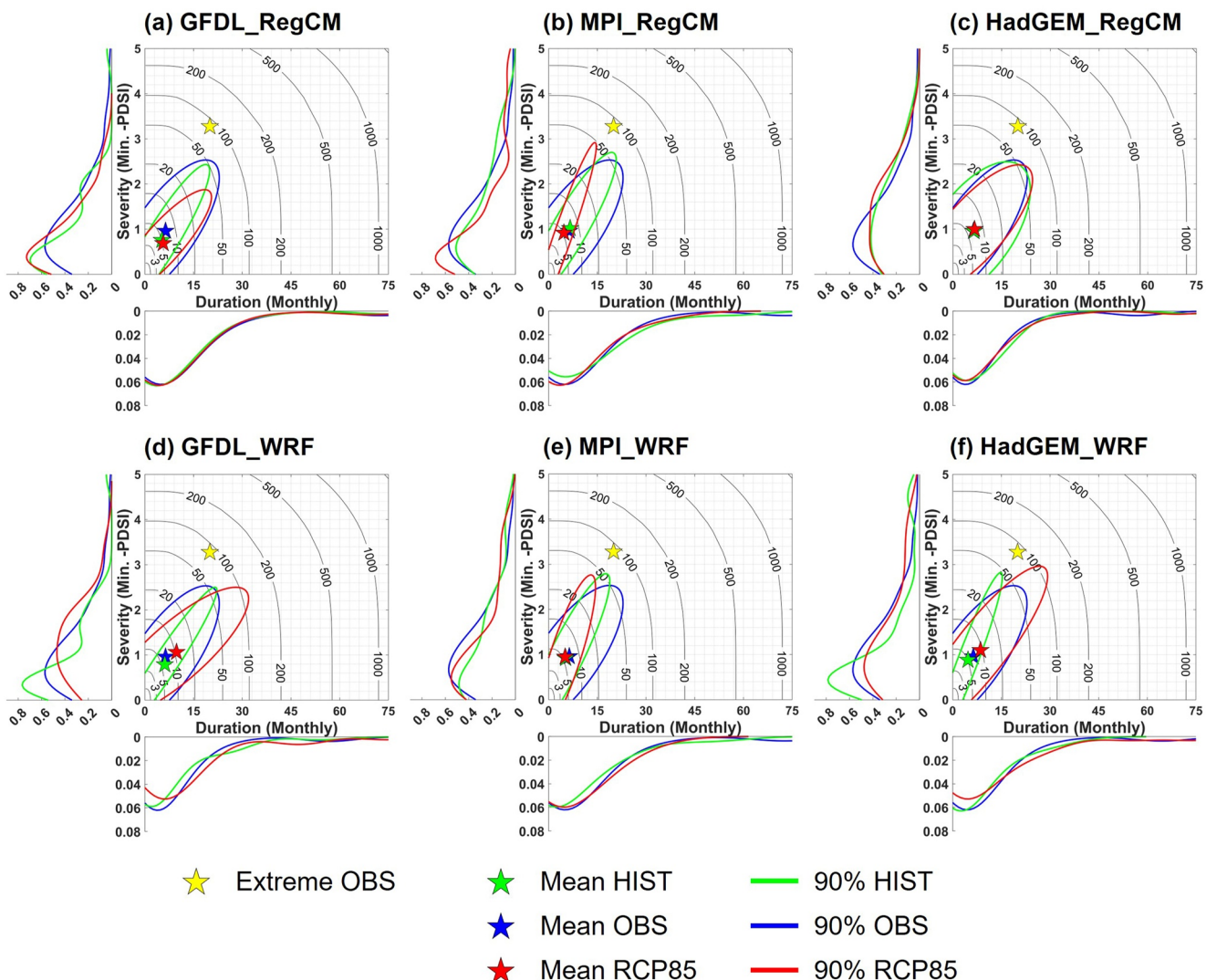


Figure 10. As in Figure 9, but for PDSI_detrended. Figure S3 in Supporting Information S1 presents the detailed distribution of each drought event as colored scatter dots (Observation-blue, Historical-green, RCP85-red).

RCP8.5 projection compared to the historical simulation, which results in reducing (enhancing) the incidence in the range of low (high) values (Figure 9). Interestingly, the drought characteristics based on SPI are quite different from PDSI_detrended, even though both indices do not show significant changes under the RCP8.5 scenario. The dependency in severity and duration of droughts constructed from SPI appears to be weaker, resulting in an expanded uncertainty in the estimation of the return period. It is also noteworthy that the severity of the current California drought for the year 2022, based on SPI, turns out to be the usual, with a joint return period not exceeding about 3 years, whereas the same event is considered statistically very rare with a return period of 100 years when measured using PDSI. This stark difference clearly highlights how much the drought characteristics depend on the choice of indices selected (IPCC, 2012). Overall, the drought risk estimation based on the index that includes temperature demonstrates that future drought will be more severe and prolonged under a warmer climate, which is not depicted if the assessment foregoes the effect of rising temperature. This finding has also been reiterated in previous studies focusing on other regions (Bonsal et al., 2013; Mesbahzadeh et al., 2020; Pathak & Dodamani, 2020; Won & Kim, 2020).

By comparing Figures 9–11, it can be seen that a structured relationship between severity and duration of droughts is shaped differently along with the indices. For the historical period, PDSI builds a strongly coupled regime, resulting in a narrow shape of the joint distribution of severity and duration. However, strong warming under the RCP8.5 scenario can significantly modulate the marginal distribution of drought severity while the effect on

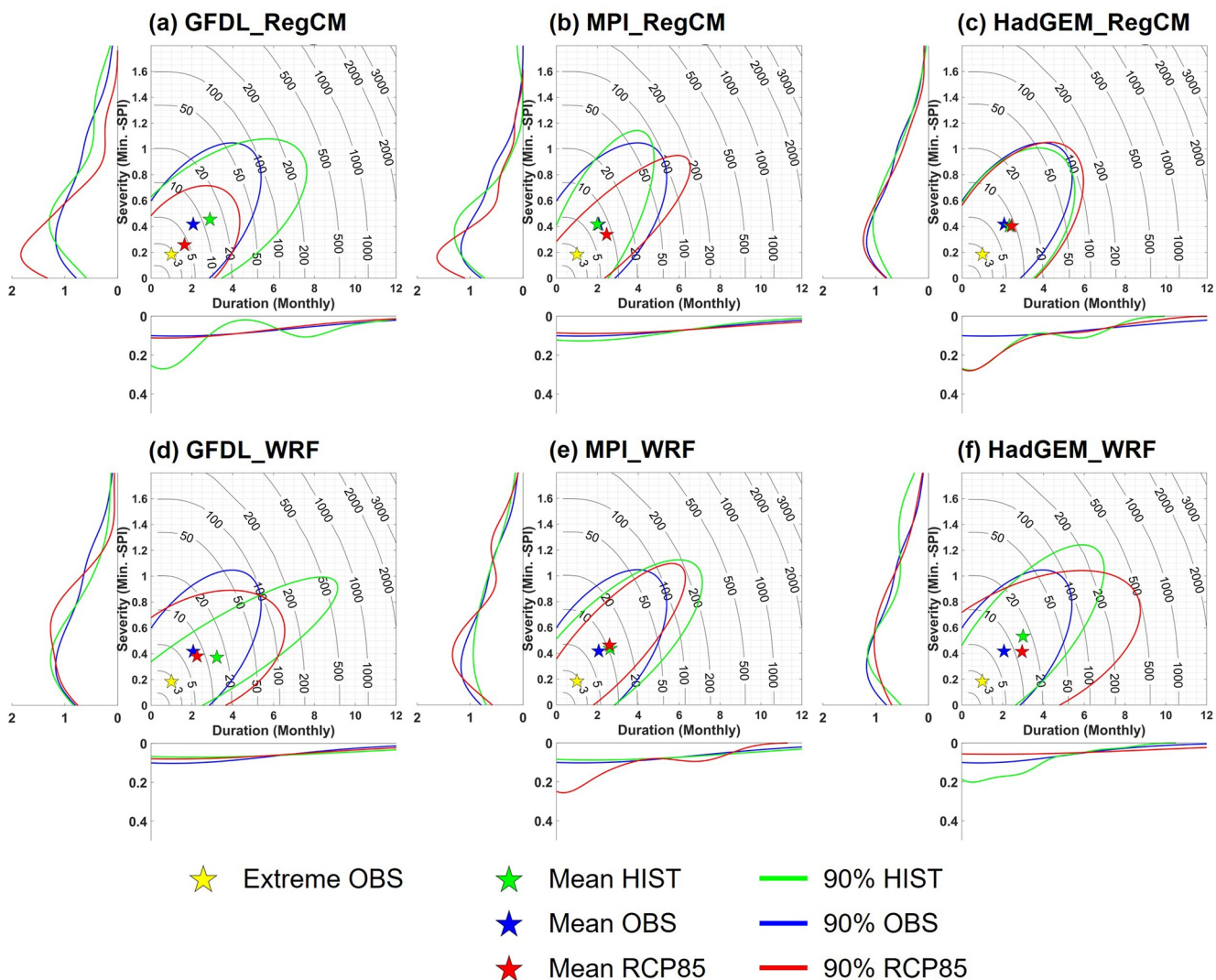


Figure 11. As in Figure 9, but for SPI. Figure S4 in Supporting Information S1 presents the detailed distribution of each drought event as colored scatter dots (Observation-blue, Historical-green, RCP85-red).

drought duration is not as pronounced. As a result, the joint structure between duration and severity may weaken, allowing for the emergence of extremely severe droughts without a prolonged drought period.

This behavior is only observed in PDSI, but not in SPI. The PDSI is based on a soil moisture balance model for the derivation of the net moisture balance so that drought severity represents the absence of soil moisture contents with physically limited soil moisture capacity. This is why the drought severity may not consistently increase, even as the drought condition extends its duration. In this perspective, the degree of warming can play a considerable role in depriving soil moisture. Meanwhile, it is equally important to scrutinize how the changes in precipitation are translated into drought characteristics. The percentage changes in precipitation appear to be mutually inconsistent over climate models under rather different warming sensitivities (Figures 6 and 7), leading to a more spread-out marginal distribution of drought severity that deviates from the joint distribution observed in the historical period.

4. Discussion

4.1. Impact of Model Selection

Although the projections of future droughts based on the conventional ensemble mean might provide the gross features dominated by the majority models (e.g., Cook et al., 2020; Ukkola et al., 2020), they could conceal

detailed characteristics of individual models. In this regard, the systematic comparisons of each model's behaviors, as done by this study, are helpful for a better interpretation of how different combinations of temperature and precipitation changes can be responsible for the joint distribution of severity and drought of meteorological droughts. However, we acknowledge that three CMIP5 projections under a single scenario (i.e., RCP8.5) may not construct the wide spectrum of temperature and precipitation changes. In addition, the latest CMIP6 models are not fully utilized due to the unavailability of CMIP6 dynamically downscaled data sets. Therefore, we compared the statistically downscaled products of CMIP5 (U.S. Department of the Interior, Bureau of Reclamation, 2013) and CMIP6 (Thrasher et al., 2022) instead to examine the impact of model selection on our results.

First, six CMIP5 models are selected based on their warming sensitivities. Figure S5 in Supporting Information S1 shows the global mean temperature anomalies of 30 CMIP5 models in 1950–2099 (covering our study period). Based on Figure S5 in Supporting Information S1, the previously selected three CMIP5 GCMs (GFDL, MPI, HadGEM) are situated in the lower, middle, and upper range of the CMIP5 model warming sensitivity. To ensure the representativeness of model warming sensitivities, we included three other models, namely GISS-E2-R (Goddard Institute for Space Studies with ModelE/Russell; lower bound of the warming sensitivity), HadGEM2-CC (Hadley Centre Global Environment Model version 2 with Carbon Cycle; upper bound of the warming sensitivity), and CESM1-BGC (Community Earth System Model version 1.0 with Biogeochemistry) to fill in the gap between MPI and GFDL. We then compared the CMIP5 models with their updated version in CMIP6 to assess the impact of model selection, as illustrated in Figures S6–S8 in Supporting Information S1. While some differences exist in the exact position of future drought return periods based on CMIP5 and CMIP6, our main finding that PDSI exclusively depicts the exacerbation of future droughts, and that the warming trend dominantly contributes to this exacerbation holds true. The presence of a fairly consistent pattern across CMIP5 and CMIP6 multiple models provides an indication that supports the robustness of the future drought projections featured in this study.

4.2. Comparison With Related Studies

Previous research has stressed the impacts of anthropogenic warming on exacerbating droughts in California, which aligns with our results. For example, Shukla et al. (2015) use a hydrologic model to analyze the 2014 California drought, and find that although low precipitation drives the drought, high temperatures play a significant role in exacerbating it. With a focus on the 2012–2014 California drought, Diffenbaugh et al. (2015) compare the drought risks with and without anthropogenic forcings, revealing that anthropogenic warming has increased the likelihood of concurrent temperature and precipitation patterns that historically led to drought in California. Williams et al. (2015) also isolate anthropogenic warming from temperature's natural variability and conclude that as human-induced warming continues, natural climate variability will become growingly insufficient to offset the drying effects of warming. Looking at a larger scope, Cook et al. (2015) project significantly drier conditions in the American Southwest and Central Plains in the latter half of the twenty-first century compared to the twentieth century and earlier paleoclimatic intervals, leading to unprecedented drought conditions during the last millennium. Seager et al. (2007) intercompare 19 CMIP3 models and demonstrate a broad model consensus in a future transition to a more arid climate in southwestern North America, suggesting that the 1950s droughts will become the new climatology (Seager et al., 2007). Collectively, these studies support our conclusion that future warming will likely establish recent severe drought as the staggering new norm.

4.3. Limitations and Future Works

Several caveats of our study should be considered. We are aware that PDSI and SPI do not sufficiently represent a full range of drought characteristics because drought is the result of a multitude of complex physical processes acting at various scales. In addition, the PDSI-embedded parameterization of PET as empirically dependent on temperature may be a proxy for actual evapotranspiration, but may not fully consider soil moisture and vegetation control related to drought development (IPCC, 2021). The effect of temperature on the wide range of drought indices across meteorological, agricultural, and hydrological drought as well as their transitions will be investigated in our future studies. While this study attempts to scrutinize the resultant effects of temperature that differentiate the joint distribution of drought severity and duration, future work will more focus on the process-oriented evaluation of drought indices in response to different levels of warming.

5. Summary and Conclusions

A significant body of research has investigated future drought projections from global to regional perspectives to understand the impact of accelerating global warming on the severity and frequency of extreme droughts (Ahmadalipour et al., 2017; Cook et al., 2014, 2015; Dai et al., 2018; Diffenbaugh et al., 2015; Lee et al., 2019). Although there is a general consensus that the intensified hydrological cycle may worsen hydroclimatic extremes such as drought (Giorgi et al., 2011), the increase in intensity and/or duration of future droughts is less reliable compared to temperature-based extremes (e.g., heatwaves) (IPCC, 2012). Besides the uncertainty that stems from the nature of precipitation, the ambiguity of the drought definition further complicates the analysis of future changes in its characteristics. These factors collectively lead to inconsistent or even contrasting results in terms of the direction of future drought changes (Burke & Brown, 2008; Cook et al., 2018; Hoffmann et al., 2020), particularly leaving room for further examination regarding the choice of drought indices and selected climate projections.

In this regard, this study characterizes future droughts by determining the joint return periods of their severity and duration using a copula model, focusing on the differences and similarities based on multiple drought indices and multi-model climate projections. The California region is targeted because an unprecedented level of mega-drought has repeatedly emerged recently (Griffin & Anchukaitis, 2014; Swain, 2015; Williams et al., 2022). Given that increased evapotranspiration under a warmer climate is regarded as the main driver of drought, a comparative assessment is conducted to explicitly discern temperature's effect on drought assessment. More specifically, two indices calculated with different principles (PDSI vs. SPI) as well as the same PDSI index but fed by different input data (original vs. detrended temperature time series) are comprehensively compared. These indices are calculated with temperature and precipitation data which are dynamically downscaled using two RCMs from three GCMs with different warming sensitivities.

The added value of fine-scale downscaled results is thoroughly evaluated by comparing temperature, precipitation, and resultant drought aspects against observation and driving GCMs during the historical period. Future changes in these three measures are also investigated. All models unequivocally project an increase in future temperature, and the amount well correlates with the driving GCM's warming sensitivity, while prospective changes in precipitation are more divergent and model-dependent. Changes in the two meteorological variables combinedly alter future drought characteristics, which are measured by three drought indices, namely, PDSI, PDSI_detrended, and SPI. Comparing the time series of these indices, only PDSI shows a clear decreasing trend in the future period, indicating the exacerbation of drought conditions due to future warming. As for the joint distribution, PDSI again exclusively depicts the higher intensity and longer duration of future droughts with long joint return periods, which have never occurred in historical simulations, whereas PDSI_detrended and SPI show minimal differentiation in drought characteristics between the historical and future periods. Since PDSI is the sole index that explicitly incorporates a warming trend, both findings substantiate the role of temperature in exacerbating droughts.

Consequently, the models' warming sensitivities, which lead to discrepant levels of temperature increase, affect PDSI-based drought projections. Our results demonstrate that models with higher warming sensitivities (hence larger temperature increases) project more intense and longer-lasting droughts in the future, even if there is a precipitation surplus. On the other hand, an aggravated precipitation deficit is needed to compensate for a lower warming magnitude and result in droughts on a comparable level. To summarize, drought intensification under future warming scenarios can be clearly revealed only when the index incorporating temperature characterizes future drought. Moreover, climate projections with higher warming sensitivity to the emission forcings unveil the changes in drought with greater clarity. Ultimately, this research highlights the uncertainty stemming from drought indices and the climate model's warming sensitivity for the assessment of future droughts.

Data Availability Statement

The downscaled meteorological data over the NA-CORDEX domain is retrieved from National Center for Atmospheric Research (NCAR) Climate Data Gateway via <https://doi.org/10.5065/D6SJ1JCH> (Mearns et al., 2017). The driving GCM data from three CMIP5 models (Taylor et al., 2012) is retrieved via <https://esgf-node.llnl.gov/projects/cmip5/>. The CRU TS v4 data is retrieved from <https://crudata.uea.ac.uk/cru/data/hrg/> (Harris et al., 2020). The PDSI, PDSI_detrended, and SPI are calculated using Matlab, and are archived in the institutional

repository at: <https://doi.org/10.14711/dataset/UGI2JW> (Zhou et al., 2023). The joint return period estimation is calculated using Matlab. Climate Data Operators is used for processing the data. The NOAA/NCEI California climate division shapefiles are downloaded from <https://psl.noaa.gov/data/usclimdivs/boundaries.html> (NOAA National Centers for Environmental Information, 2023). The statistically downscaled CMIP5 data was retrieved from <https://gdo-dcp.ucrlnl.org/> (U.S. Department of the Interior, Bureau of Reclamation, 2013). The statistically downscaled CMIP6 data is from National Aeronautics and Space Administration (NASA) Earth Exchange Global Daily Downscaled Projections (Thrasher et al., 2022) at <https://nex-gddp-cmip6.s3.us-west-2.amazonaws.com/index.html#NEX-GDDP-CMIP6/>.

Acknowledgments

This work was supported by Korea Environmental Industry & Technology Institute through Water Management Program for Drought Project, funded by Korea Ministry of Environment (2022003610003). Additionally, Im E.S. and Zhou Z. were partly supported by the Hong Kong Research Grants Council-funded project, GRF16308722. The authors acknowledge all of the modeling teams that contributed to NA-CORDEX, CMIP5, and statistically downscaled CMIP5 and CMIP6 data.

References

- Abatzoglou, J. T. (2013). Development of gridded surface meteorological data for ecological applications and modelling. *International Journal of Climatology*, 33(1), 121–131. <https://doi.org/10.1002/joc.3413>
- AghaKouchak, A., Cheng, L., Mazdiyasni, O., & Farahmand, A. (2014). Global warming and changes in risk of concurrent climate extremes: Insights from the 2014 California drought. *Geophysical Research Letters*, 41(24), 8847–8852. <https://doi.org/10.1002/2014GL062308>
- Ahmadalipour, A., Moradkhani, H., & Svoboda, M. (2017). Centennial drought outlook over the CONUS using NASA-NEX downscaled climate ensemble. *International Journal of Climatology*, 37(5), 2477–2491. <https://doi.org/10.1002/joc.4859>
- Allen, R. J., & Anderson, R. G. (2018). 21st century California drought risk linked to model fidelity of the El Niño teleconnection. *Npj Climate and Atmospheric Science*, 1(1), 21. <https://doi.org/10.1038/s41612-018-0032-x>
- Becker, R. (2022). Four in a row: California drought likely to continue. *The Mercury News*. Retrieved from <https://www.mercurynews.com/2022/09/28/four-in-a-row-california-drought-likely-to-continue/>
- Beniston, M., Stephenson, D. B., Christensen, O. B., Ferro, C. A. T., Frei, C., Goyette, S., et al. (2007). Future extreme events in European climate: An exploration of regional climate model projections. *Climatic Change*, 81(S1), 71–95. <https://doi.org/10.1007/s10584-006-9226-z>
- Bonsal, B. R., Aider, R., Gachon, P., & Lapp, S. (2013). An assessment of Canadian prairie drought: Past, present, and future. *Climate Dynamics*, 41(2), 501–516. <https://doi.org/10.1007/s00382-012-1422-0>
- Bukovsky, M. S., & Mearns, L. O. (2020). Regional climate change projections from NA-CORDEX and their relation to climate sensitivity. *Climatic Change*, 162(2), 645–665. <https://doi.org/10.1007/s10584-020-02835-x>
- Burke, E. J., & Brown, S. J. (2008). Evaluating uncertainties in the projection of future drought. *Journal of Hydrometeorology*, 9(2), 292–299. <https://doi.org/10.1175/2007JHM929.1>
- Burke, E. J., Brown, S. J., & Christidis, N. (2006). Modeling the recent evolution of global drought and projections for the twenty-first century with the Hadley Centre climate model. *Journal of Hydrometeorology*, 7(5), 1113–1125. <https://doi.org/10.1175/jhm544.1>
- Cai, W., Cowan, T., Briggs, P., & Raupach, M. (2009). Rising temperature depletes soil moisture and exacerbates severe drought conditions across southeast Australia. *Geophysical Research Letters*, 36(21), L21709. <https://doi.org/10.1029/2009GL040334>
- California Department of Water Resources. (2022a). New water year begins amid preparations for continued drought. Retrieved from <https://water.ca.gov/News/News-Releases/2022/Oct-22/New-Water-Year-Begins-Amid-Preparations-for-Continued-Drought>
- California Department of Water Resources. (2022b). Survey finds little snow as statewide snowpack drops to 38 percent following record dry months. Retrieved from <https://water.ca.gov/News/News-Releases/2022/April-22/April-2022-Snow-Survey>
- Cannon, A. J. (2018). Multivariate quantile mapping bias correction: An N-dimensional probability density function transform for climate model simulations of multiple variables. *Climate Dynamics*, 50(1–2), 31–49. <https://doi.org/10.1007/s00382-017-3580-6>
- Collins, W. J., Bellouin, N., Doutriaux-Boucher, M., Gedney, N., Halloran, P., Hinton, T., et al. (2011). Development and evaluation of an Earth-System model – HadGEM2. *Geoscientific Model Development*, 4(4), 1051–1075. <https://doi.org/10.5194/gmd-4-1051-2011>
- Cook, B. I., Ault, T. R., & Smerdon, J. E. (2015). Unprecedented 21st century drought risk in the American Southwest and Central Plains. *Science Advances*, 1(1). <https://doi.org/10.1126/sciadv.1400082>
- Cook, B. I., Mankin, J. S., & Anchukaitis, K. J. (2018). Climate change and drought: From past to future. *Current Climate Change Reports*, 4(2), 164–179. <https://doi.org/10.1007/s40641-018-0093-2>
- Cook, B. I., Mankin, J. S., Marvel, K., Williams, A. P., Smerdon, J. E., & Anchukaitis, K. J. (2020). Twenty-first century drought projections in the CMIP6 forcing scenarios. *Earth's Future*, 8(6). <https://doi.org/10.1029/2019EF001461>
- Cook, B. I., Smerdon, J. E., Seager, R., & Coats, S. (2014). Global warming and 21st century drying. *Climate Dynamics*, 43(9–10), 2607–2627. <https://doi.org/10.1007/s00382-014-2075-y>
- Dai, A. (2011). Drought under global warming: A review. *Wiley Interdisciplinary Reviews: Climate Change*, 2(1), 45–65. <https://doi.org/10.1002/wcc.81>
- Dai, A. (2013). Increasing drought under global warming in observations and models. *Nature Climate Change*, 3(1), 52–58. <https://doi.org/10.1038/nclimate1633>
- Dai, A., Trenberth, K. E., & Qian, T. (2004). A global dataset of Palmer Drought Severity Index for 1870–2002: Relationship with soil moisture and effects of surface warming. *Journal of Hydrometeorology*, 5(6), 1117–1130. <https://doi.org/10.1175/JHM-386.1>
- Dai, A., Zhao, T., & Chen, J. (2018). Climate change and drought: A precipitation and evaporation perspective. *Current Climate Change Reports*, 4(3), 301–312. <https://doi.org/10.1007/s40641-018-0101-6>
- Diffenbaugh, N. S., Swain, D. L., & Touma, D. (2015). Anthropogenic warming has increased drought risk in California. *Proceedings of the National Academy of Sciences*, 112(13), 3931–3936. <https://doi.org/10.1073/pnas.1422385112>
- Dunne, J. P., John, J. G., Adcroft, A. J., Griffies, S. M., Hallberg, R. W., Shevliakova, E., et al. (2012). GFDL's ESM2 global coupled climate–carbon earth system models. Part I: Physical formulation and baseline simulation characteristics. *Journal of Climate*, 25(19), 6646–6665. <https://doi.org/10.1175/jcli-d-11-00560.1>
- Dunne, J. P., John, J. G., Shevliakova, E., Stouffer, R. J., Krasting, J. P., Malyshov, S. L., et al. (2013). GFDL's ESM2 global coupled climate–carbon earth system models. Part II: Carbon system formulation and baseline simulation characteristics. *Journal of Climate*, 26(7), 2247–2267. <https://doi.org/10.1175/jcli-d-12-00150.1>
- Easterling, D. R., Wallis, T. W. R., Lawrimore, J. H., & Heim, R. R. (2007). Effects of temperature and precipitation trends on U.S. drought. *Geophysical Research Letters*, 34(20), L20709. <https://doi.org/10.1029/2007GL031541>
- Flynn, C. M., & Mauritsen, T. (2020). On the climate sensitivity and historical warming evolution in recent coupled model ensembles. *Atmospheric Chemistry and Physics*, 20(13), 7829–7842. <https://doi.org/10.5194/acp-20-7829-2020>

- Giorgetta, M. A., Jungclaus, J., Reick, C. H., Legutke, S., Bader, J., Böttinger, M., et al. (2013). Climate and carbon cycle changes from 1850 to 2100 in MPI-ESM simulations for the Coupled Model Intercomparison Project phase 5: Climate changes in MPI-ESM. *Journal of Advances in Modeling Earth Systems*, 5(3), 572–597. <https://doi.org/10.1002/jame.20038>
- Giorgi, F., Coppola, E., Jacob, D., Teichmann, C., Abba Omar, S., Ashfaq, M., et al. (2021). The CORDEX-CORE EXP-I initiative: Description and highlight results from the initial analysis. *Bulletin of the American Meteorological Society*, 1–52.
- Giorgi, F., Coppola, E., Solmon, F., Mariotti, L., Sylla, M. B., Bi, X., et al. (2012). RegCM4: Model description and preliminary tests over multiple CORDEX domains. *Climate Research*, 52, 7–29. <https://doi.org/10.3354/cr01018>
- Giorgi, F., & Gutowski, W. J. (2016). Coordinated experiments for projections of regional climate change. *Current Climate Change Reports*, 2(4), 202–210. <https://doi.org/10.1007/s40641-016-0046-6>
- Giorgi, F., Im, E.-S., Coppola, E., Diffenbaugh, N. S., Gao, X. J., Mariotti, L., & Shi, Y. (2011). Higher hydroclimatic intensity with global warming. *Journal of Climate*, 24(20), 5309–5324. <https://doi.org/10.1175/2011JCLI3979.1>
- Griffin, D., & Anchukaitis, K. J. (2014). How unusual is the 2012–2014 California drought? *Geophysical Research Letters*, 41(24), 9017–9023. <https://doi.org/10.1002/2014GL062433>
- Harris, I., Osborn, T. J., Jones, P., & Lister, D. (2020). Version 4 of the CRU TS monthly high-resolution gridded multivariate climate dataset [Dataset]. <https://doi.org/10.1038/s41597-020-0453-3>
- Hawkins, E., & Sutton, R. (2009). The potential to narrow uncertainty in regional climate predictions. *Bulletin of the American Meteorological Society*, 90(8), 1095–1108. <https://doi.org/10.1175/2009BAMS2607.1>
- He, M., & Gautam, M. (2016). Variability and trends in precipitation, temperature and drought indices in the state of California. *Hydrology*, 3(2), 14. <https://doi.org/10.3390/hydrology302004>
- Hoffmann, D., Gallant, A. J. E., & Arblaster, J. M. (2020). Uncertainties in drought from index and data selection. *Journal of Geophysical Research: Atmospheres*, 125(18). <https://doi.org/10.1029/2019JD031946>
- Houghton, J. T., Ding, Y., Griggs, D. J., Noguer, M., van der Linden, P. J., Dai, X., et al. (2001). *Climate change 2001: The scientific basis: Contribution of Working Group I to the third assessment report of the Intergovernmental Panel on Climate Change*. Cambridge University Press.
- Hughes, M., Swales, D., Scott, J. D., Alexander, M., Mahoney, K., McCrary, R. R., et al. (2022). Changes in extreme integrated water vapor transport on the U.S. west coast in NA-CORDEX, and relationship to mountain and inland precipitation. *Climate Dynamics*, 59(3–4), 973–995. <https://doi.org/10.1007/s00382-022-06168-6>
- Im, E.-S., Ahn, J.-B., & Kim, D.-W. (2012). An assessment of future dryness over Korea based on the ECHAM5-RegCM3 model chain under A1B emission scenario. *Asia-Pacific Journal of Atmospheric Sciences*, 48(4), 325–337. <https://doi.org/10.1007/s13143-012-0031-5>
- IPCC. (2012). In C. B. Field, V. Barros, T. F. Stocker, D. Qin, D. J. Dokken, et al. (Eds.), *Managing the risks of extreme events and disasters to advance climate change adaptation. A Special Report of Working Groups I and II of the Intergovernmental Panel on Climate Change* (p. 582). Cambridge University Press.
- IPCC. (2021). In V. Masson-Delmotte, P. Zhai, A. Pirani, S. L. Connors, C. Péan, et al. (Eds.), *Climate change 2021: The physical science basis. Contribution of Working Group I to the sixth assessment report of the Intergovernmental Panel on Climate Change*. Cambridge University Press. <https://doi.org/10.1017/9781009157896>
- Kelley, C. P., Mohtadi, S., Cane, M. A., Seager, R., & Kushnir, Y. (2015). Climate change in the Fertile Crescent and implications of the recent Syrian drought. *Proceedings of the National Academy of Sciences*, 112(11), 3241–3246. <https://doi.org/10.1073/pnas.1421533112>
- Kew, S. F., Philip, S. Y., Hauser, M., Hobbins, M., Wanders, N., van Oldenborgh, G. J., et al. (2021). Impact of precipitation and increasing temperatures on drought trends in eastern Africa. *Earth System Dynamics*, 12(1), 17–35. <https://doi.org/10.5194/esd-12-17-2021>
- Kim, S., Eghdamirad, S., Sharma, A., & Kim, J. H. (2020). Quantification of uncertainty in projections of extreme daily precipitation. *Earth and Space Science*, 7(8). <https://doi.org/10.1029/2019EA001052>
- Knutti, R., Stocker, T. F., Joos, F., & Plattner, G.-K. (2002). Constraints on radiative forcing and future climate change from observations and climate model ensembles. *Nature*, 416(6882), 719–723. <https://doi.org/10.1038/416719a>
- Lee, M.-H., Im, E.-S., & Bae, D.-H. (2019). A comparative assessment of climate change impacts on drought over Korea based on multiple climate projections and multiple drought indices. *Climate Dynamics*, 53(1–2), 389–404. <https://doi.org/10.1007/s00382-018-4588-2>
- Lehner, F., Coats, S., Stocker, T. F., Pendergrass, A. G., Sanderson, B. M., Raible, C. C., & Smerdon, J. E. (2017). Projected drought risk in 1.5°C and 2°C warmer climates. *Geophysical Research Letters*, 44(14), 7419–7428. <https://doi.org/10.1029/2017GL074117>
- Luo, L., Apps, D., Arcand, S., Xu, H., Pan, M., & Hoerling, M. (2017). Contribution of temperature and precipitation anomalies to the California drought during 2012–2015. *Geophysical Research Letters*, 44(7), 3184–3192. <https://doi.org/10.1002/2016GL072027>
- Magan, B., Kim, S., Wasko, C., Barbero, R., Moron, V., Nathan, R., & Sharma, A. (2020). Impact of atmospheric circulation on the rainfall-temperature relationship in Australia. *Environmental Research Letters*, 15(9), 094098. <https://doi.org/10.1088/1748-9326/abab35>
- Mao, Y., Nijssen, B., & Lettenmaier, D. P. (2015). Is climate change implicated in the 2013–2014 California drought? A hydrologic perspective. *Geophysical Research Letters*, 42(8), 2805–2813. <https://doi.org/10.1002/2015GL063456>
- McKee, T. B., Doesken, N. J., & Kleist, J. (1993). The relationship of drought frequency and duration to time scales. *Proceedings of the 8th Conference on Applied Climatology*, 17, 179–183.
- Mearns, L. O., McGinnis, S., Korytina, D., Arritt, R., Biner, S., Bukovsky, M., et al. (2017). The NA-CORDEX dataset, version 1.0 [Dataset]. <https://doi.org/10.5065/D6SJ1JCH>
- Mesbahzadeh, T., Mirakbari, M., Mohseni Saravi, M., Soleimani Sardoo, F., & Miglietta, M. M. (2020). Meteorological drought analysis using copula theory and drought indicators under climate change scenarios (RCP). *Meteorological Applications*, 27(1). <https://doi.org/10.1002/met.1856>
- Meyer, J. D. D., Wang, S.-Y. S., Gillies, R. R., & Yoon, J. (2021). Evaluating NA-CORDEX historical performance and future change of western U.S. precipitation patterns and modes of variability. *International Journal of Climatology*, 41(9), 4509–4532. <https://doi.org/10.1002/joc.7083>
- National Drought Mitigation Center, National Oceanic and Atmospheric Administration, & U.S. Department of Agriculture. (2022). Current U.S. drought monitor conditions for California. Retrieved from <https://www.drought.gov/states/california#current-conditions>
- National Oceanic and Atmospheric Administration & National Integrated Drought Information System. (2022). Western regional climate center quarterly impacts and outlook – Summer 2022. Retrieved from <https://www.drought.gov/documents/quarterly-climate-impacts-and-outlook-western-region-september-2022>
- NOAA National Centers for Environmental Information. (2023). NOAA/NCEI U.S. Climate Division Data Plotting Page: Division boundaries and county relationships [Dataset]. <https://psl.noaa.gov/data/usclimdivs/boundaries.html>
- Palmer, W. C. (1965). *Meteorological drought* (Vol. 30). US Department of Commerce.
- Pathak, A. A., & Dodamani, B. M. (2020). Comparison of meteorological drought indices for different climatic regions of an Indian river basin. *Asia-Pacific Journal of Atmospheric Sciences*, 56(4), 563–576. <https://doi.org/10.1007/s13143-019-00162-5>

- Qiu, L., & Im, E.-S. (2021). Added value of high-resolution climate projections over South Korea on the scaling of precipitation with temperature. *Environmental Research Letters*, 16(12), 124034. <https://doi.org/10.1088/1748-9326/ac37d3>
- Qiu, L., Im, E.-S., Hur, J., & Shim, K.-M. (2020). Added value of very high resolution climate simulations over South Korea using WRF modeling system. *Climate Dynamics*, 54(1–2), 173–189. <https://doi.org/10.1007/s00382-019-04992-x>
- Räisänen, J. (2007). How reliable are climate models? *Tellus A: Dynamic Meteorology and Oceanography*, 59(1), 2. <https://doi.org/10.1111/j.1600-0870.2006.00211.x>
- Reyniers, N., Osborn, T. J., Addor, N., & Darch, G. (2023). Projected changes in droughts and extreme droughts in Great Britain strongly influenced by the choice of drought index. *Hydrology and Earth System Sciences*, 27(5), 1151–1171. <https://doi.org/10.5194/hess-27-1151-2023>
- Rhee, J., & Cho, J. (2016). Future changes in drought characteristics: Regional analysis for South Korea under CMIP5 projections. *Journal of Hydrometeorology*, 17(1), 437–451. <https://doi.org/10.1175/JHM-D-15-0027.1>
- Rind, D., Goldberg, R., Hansen, J., Rosenzweig, C., & Ruedy, R. (1990). Potential evapotranspiration and the likelihood of future drought. *Journal of Geophysical Research*, 95(D7), 9983–10004. <https://doi.org/10.1029/JD095iD07p09983>
- Satoh, Y., Shiogama, H., Hanasaki, N., Pokhrel, Y., Boulange, J. E. S., Burek, P., et al. (2021). A quantitative evaluation of the issue of drought definition: A source of disagreement in future drought assessments. *Environmental Research Letters*, 16(10), 104001. <https://doi.org/10.1088/1748-9326/ac2348>
- Seager, R., Ting, M., Held, I., Kushnir, Y., Lu, J., Vecchi, G., et al. (2007). Model projections of an imminent transition to a more arid climate in southwestern North America. *Science*, 316(5828), 1181–1184. <https://doi.org/10.1126/science.1139601>
- Sheffield, J., Wood, E. F., & Roderick, M. L. (2012). Little change in global drought over the past 60 years. *Nature*, 491(7424), 435–438. <https://doi.org/10.1038/nature11575>
- Shukla, S., Safeeq, M., Aghakouchak, A., Guan, K., & Funk, C. (2015). Temperature impacts on the water year 2014 drought in California. *Geophysical Research Letters*, 42(11), 4384–4393. <https://doi.org/10.1002/2015GL063666>
- Skamarock, W. C., Klemp, J. B., Dudhia, J., Gill, D. O., Liu, Z., Berner, J., et al. (2019). *A description of the advanced research WRF model version 4*. UCAR/NCAR. <https://doi.org/10.5065/1DFH-6P97>
- Stagge, J. H., Tallaksen, L. M., Gudmundsson, L., Van Loon, A. F., & Stahl, K. (2015). Candidate distributions for climatological drought indices (SPI and SPEI). *International Journal of Climatology*, 35(13), 4027–4040. <https://doi.org/10.1002/joc.4267>
- Sutanto, S. J., & Van Lanen, H. A. J. (2021). Streamflow drought: Implication of drought definitions and its application for drought forecasting. *Hydrology and Earth System Sciences*, 25(7), 3991–4023. <https://doi.org/10.5194/hess-25-3991-2021>
- Swain, D. L. (2015). A tale of two California droughts: Lessons amidst record warmth and dryness in a region of complex physical and human geography: A tale of two California droughts. *Geophysical Research Letters*, 42(22), 9999–10003. <https://doi.org/10.1002/2015GL066628>
- Taylor, K. E., Stouffer, R. J., & Meehl, G. A. (2012). An overview of CMIP5 and the experiment design. *Bulletin of the American Meteorological Society*, 93(4), 485–498. <https://doi.org/10.1175/bams-d-11-00094.1>
- Teichmann, C., Jacob, D., Remedio, A. R., Remke, T., Buntemeyer, L., Hoffmann, P., et al. (2021). Assessing mean climate change signals in the global CORDEX-CORE ensemble. *Climate Dynamics*, 57(5–6), 1269–1292. <https://doi.org/10.1007/s00382-020-05494-x>
- The California Natural Resources Agency, The California Environmental Protection Agency, The Governor's Office of Emergency Services, The California Department of Food and Agriculture, The Department of Water Resources, The Department of Fish and Wildlife, et al. (2022). California drought update.
- Thornthwaite, C. W. (1948). An approach toward a rational classification of climate. *Geographical Review*, 38(1), 55–94. <https://doi.org/10.2307/210739>
- Thrasher, B., Wang, W., Michaelis, A., Melton, F., Lee, T., & Nemani, R. (2022). NASA global daily downscaled projections, CMIP6 [Dataset]. <https://doi.org/10.1038/s41597-022-01393-4>
- Tie, J., Kim, S., & Sharma, A. (2023). How does increasing temperature affect the sub-annual distribution of monthly rainfall? *Environmental Research: Climate*, 2(1), 015004. <https://doi.org/10.1088/2752-5295/acb5b9>
- Touma, D., Ashfaq, M., Nayak, M. A., Kao, S.-C., & Diffenbaugh, N. S. (2015). A multi-model and multi-index evaluation of drought characteristics in the 21st century. *Journal of Hydrology*, 526, 196–207. <https://doi.org/10.1016/j.jhydrol.2014.12.011>
- Trenberth, K. E., Dai, A., van der Schrier, G., Jones, P. D., Barichivich, J., Briffa, K. R., & Sheffield, J. (2014). Global warming and changes in drought. *Nature Climate Change*, 4(1), 17–22. <https://doi.org/10.1038/nclimate2067>
- Trenberth, K. E., Jones, P. D., Ambenje, P., Bojariu, R., Easterling, D., Klein Tank, A., et al. (2007). Observations. Surface and atmospheric climate change. Chapter 3.
- Ukkola, A. M., De Kauwe, M. G., Roderick, M. L., Abramowitz, G., & Pitman, A. J. (2020). Robust future changes in meteorological drought in CMIP6 projections despite uncertainty in precipitation. *Geophysical Research Letters*, 47(11). <https://doi.org/10.1029/2020GL087820>
- U.S. Department of Agriculture. (2022). U.S. rice imports in 2022/23 are projected at an all-time high. Retrieved from <https://www.ers.usda.gov/data-products/chart-gallery/gallery/chart-detail/?chartId=104751>
- U.S. Department of the Interior, Bureau of Reclamation. (2013). Downscaled CMIP3 and CMIP5 climate projections release of downscaled CMIP5 climate projections, comparison with preceding information, and summary of user needs [Dataset]. http://gdo-dcp.ucar.edu/downscaled_cmip_projections/techmemo/downscaled_climate.pdf
- Van der Schrier, G., Jones, P., & Briffa, K. (2011). The sensitivity of the PDSI to the Thornthwaite and Penman-Monteith parameterizations for potential evapotranspiration. *Journal of Geophysical Research*, 116(D3), D03106. <https://doi.org/10.1029/2010jd015001>
- Walton, D., Berg, N., Pierce, D., Maurer, E., Hall, A., Lin, Y., et al. (2020). Understanding differences in California climate projections produced by dynamical and statistical downscaling. *Journal of Geophysical Research: Atmospheres*, 125(19), e2020JD032812. <https://doi.org/10.1029/2020JD032812>
- Williams, A. P., Cook, B. I., & Smerdon, J. E. (2022). Rapid intensification of the emerging southwestern North American megadrought in 2020–2021. *Nature Climate Change*, 12(3), 232–234. <https://doi.org/10.1038/s41558-022-01290-z>
- Williams, A. P., Seager, R., Abatzoglou, J. T., Cook, B. I., Smerdon, J. E., & Cook, E. R. (2015). Contribution of anthropogenic warming to California drought during 2012–2014. *Geophysical Research Letters*, 42(16), 6819–6828. <https://doi.org/10.1002/2015GL064924>
- Won, J., & Kim, S. (2020). Future drought analysis using SPI and EDDI to consider climate change in South Korea. *Water Supply*, 20(8), 3266–3280. <https://doi.org/10.2166/ws.2020.209>
- Yang, Q., Li, M., Zheng, Z., & Ma, Z. (2017). Regional applicability of seven meteorological drought indices in China. *Science China Earth Sciences*, 60(4), 745–760. <https://doi.org/10.1007/s11430-016-5133-5>
- Zhou, Z., Kim, Y., Im, E., & Kwon, H. (2023). Drought indices derived from NA-CORDEX data [Dataset]. DataSpace@HKUST. <https://doi.org/10.14711/dataset/UG12JW>